Prediction of measurable two-dimensional plasmons in Li-intercalated graphene LiC_2

Marušić, Leonardo; Despoja, Vito

PHYSICAL REVIEW B **95**, 201408(R) (2017)

Prediction of measurable two-dimensional plasmons in Li-intercalated graphene LiC_2

L. Marušić[1,*] and V. Despoja[2,3,†]

[1]*Maritime Department, University of Zadar, M. Pavlinovića 1, HR-23000 Zadar, Croatia*

[2]*Department of Physics, Faculty of Science, University of Zagreb, Bijenička 32, HR-10000 Zagreb, Croatia*

[3]*Donostia International Physics Center (DIPC), P. Manuel de Lardizabal, 4, 20018 San Sebastián, Spain*

(Received 7 December 2016; published 11 May 2017)

The electron excitation spectra of the Li-intercalated graphene (LiC_2) are obtained using a high-accuracy *ab initio* density function theory calculation within the random phase approximation. The low-energy parts of the spectra are analyzed to predict the existence of two quasi-two-dimensional collective modes: a Dirac plasmon similar to the one in the doped graphene but significantly stronger, and an acoustic plasmon.

DOI: 10.1103/PhysRevB.95.201408

The graphenelike quasi-two-dimensional (q2D) materials, such as alkaline or alkaline-earth intercalated graphene have recently been extensively studied theoretically and experimentally, but so far the most attention has been paid to the investigation of their superconductivity, quasiparticle or ground state electronic properties, and structural stability [1–7]. However, the electronic excitations and optical properties of these materials have not been studied at all. The electronic structure suggests that they naturally support 2D plasmons which produce a strong evanescent field, making the measurement more feasible. This suggests the possibility for application of these plasmons in nanodevices operating in the terahertz to mid-infrared frequency range [8–11]. In addition, studies of other graphene-based multilayer materials, such as the graphene nanoribbons [12], the twisted graphene bilayer [13], or the graphene/SiC [14] suggest the existence of a variety of 2D plasmons or (hybridized) plasmon/phonon modes, but the experimental observation is very difficult [15], either because of the very small doping or because of the difficult experimental feasibility and the low structural stability of such systems. We chose lithium, rather than any other alkaline or alkaline-earth metal, because of its relative simplicity, and we chose full coverage rather than, e.g., 2×2 because it is experimentally more stable, and it provides higher doping.

The system we study is a LiC_2 monolayer (ML), consisting of lithium intercalated to a single graphene layer with full coverage. Adding lithium to graphene causes natural doping, lifting the Fermi level above the Dirac point, and turning the graphene layer from a gapless semiconductor into a metal. The metallic layer donates s electrons to the graphene π^* band in a way that the s band remains partially filled and the graphene cone becomes doped. This results in the formation of two thin, i.e., q2D, plasmas which can support a variety of different modes with electrostatically tunable frequencies that do not exist in the pristine graphene.

The two-dimensional plasmon (with a $\sqrt{2E_F Q}$ dispersion in the long-wavelength limit) supported in the doped graphene and referred to as a Dirac plasmon (DP), has been the subject of many theoretical discussions [8,16,17], but the experimental observation has proven to be difficult because of its low intensity. For example, the measurements performed for the graphene on SiO_2 substrate [18] proved the existence of the DP indirectly, through its influence to the phonons in the substrate, while the measurements performed for the graphene nanoribbons on SiO_2 [19] resulted with the observation of the hybrid plasmon-phonon modes. However, in this case, due to the high natural doping, the theoretically obtained intensities of the 2D plasmon modes suggest the possibility for their experimental detection and potential application, and early indications of their experimental signature have been observed [20]. This system is additionally attractive because, due to the presence of the second 2D plasma lying in lithium plane, this system supports another 2D plasmon which couples with the Dirac plasmon and takes acousticlike behavior. The phenomenon of the coexistence of two 2D plasmas separated by only ~ 0.1 nm has not been experimentally detected yet, so this theoretical investigation encourages such measurements, given that the fabrication of this system is already experimentally feasible.

In this Rapid Communication we calculate the dynamically screened Coulomb interaction, W, in the LiC_2-ML using first-principle density functional theory (DFT) within the random phase approximation (RPA), and use its imaginary part to obtain the electronic excitation spectra. By scanning the intensities of the energy dissipation peaks for each (Q,ω) electronic mode, we obtain a map of excitations. The high accuracy of the calculation enables us to focus on the low-energy region, with special emphasis on the long-wavelength limit. The dominant modes in this part of the spectra are two 2D plasmons, one in-phase, with a dispersion consistent with the DP in the doped graphene, and one in-antiphase, with a linear dispersion characteristic for the acoustic modes. Similar modes have been analyzed in the topological insulator films [21] but the acoustic mode was not observed because it is strongly Landau damped. Identification of these modes is supported by a simple semiclassical two 2D plasma model. A DP of this strength is interesting because it could enable the sensing of the molecular excitons when their energy matches the horizontal part of the DP dispersion curve [22,23]. The acoustic plasmon (AP) has been theoretically predicted [24], experimentally observed [25], and obtained by the *ab initio* calculations [26] for various metallic surfaces, while here it is obtained by very accurate *ab initio* calculations for an existing q2D system, which has recently been synthesized for experimental observation [2,7]. The tuning of the AP slope (simply by the use of an external gate voltage) opens up a

*lmarusic@unizd.hr

†vito@phy.hr

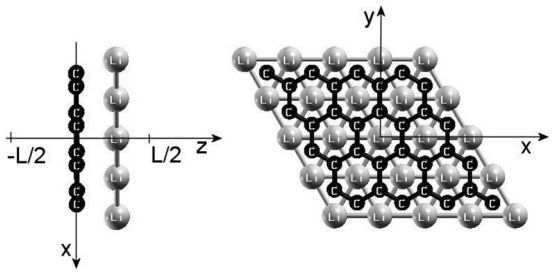

FIG. 1. The schematic representation of the LiC_2-ML. The unit-cell parameter in the parallel direction is $a = 4.651$ a.u., and the supercell parameter in the perpendicular direction is $L = 5a$.

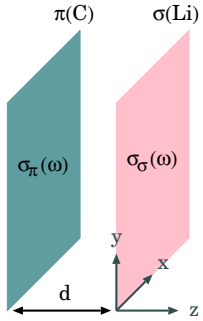

FIG. 2. Schematic representation of two 2D conducting plates separated by distance d and described by conductivities $\sigma_\pi(\omega)$ and $\sigma_\sigma(\omega)$, representing graphene and lithium planes.

remarkable opportunity for optical switching, i.e., photon-plasmon conversion, crucial for optoelectronics [27]. This is usually done by adjusting the optical grating lattice constant to make the scattered plasmon wave vector fit the photon dispersion [28], while in this system the matching is achieved simply by tuning the AP slope for the fixed grating lattice constant.

Our system is schematically shown in Fig. 1. The theoretical formulation of the electronic response in various q2D systems has already been presented [16,29–31], so here we only present a brief reminder of the method, and point out some features of the calculation characteristic for this particular system.

The first part of the calculation consists of determining the Kohn-Sham (KS) wave functions $\phi_{n\mathbf{K}}$ and energy levels $E_{n\mathbf{K}}$, i.e., the band structure, of a LiC_2-ML. For the calculation of the KS states we use the plane-wave self-consistent field DFT code (PWSCF) within the QUANTUM ESPRESSO (QE) package [32]. The core-electron interaction is approximated by the norm-conserving pseudopotentials [33], and the exchange correlation potential by the Perdew-Zunger local density approximation [34]. For the LiC_2-ML unit-cell constant we use the experimental value of $a_{uc} = 4.651$ a.u. [35], and we separate the LiC_2 monolayers by $L = 5a_{uc} = 23.255$ a.u. The equilibrium separation between the Li and C layers is 4.1 a.u. (2.17 Å), as proposed in Ref. [7]. The ground-state electronic densities of the LiC_2-ML is calculated by using the $12 \times 12 \times 1$ Monkhorst-Pack K-point mesh [36] of the first Brillouin zone (BZ), i.e., we use 19 special points in the irreducible BZ. For the plane-wave cut-off energy we choose 50 Ry (680 eV).

We define the electron energy loss spectroscopy local spectral function as

$$S_{z_0}(\mathbf{Q},\omega) = -\mathrm{Im}W_{\mathbf{G}_\parallel=0}(\mathbf{Q},\omega,z_0,z_0). \tag{1}$$

In addition to being a function of frequencies (ω) and wave vectors ($\mathbf{Q}$), the spectral function is also position dependent (local), since in principle it does depend on the position of the probe. Here the dynamically screened Coulomb interaction has the form [37] $W = v + v \otimes \chi^0 \otimes W$, where v is the bare Coulomb interaction and χ^0 is the noninteracting electrons response function:

$$\chi^0_{\mathbf{G}\mathbf{G}'}(\mathbf{Q},\omega) = \frac{2}{\Omega} \sum_{\mathbf{K}\in SBZ,n,m} \frac{f^n_{\mathbf{K}} - f^m_{\mathbf{K}+\mathbf{Q}}}{\omega + i\eta + E^n_{\mathbf{K}} - E^m_{\mathbf{K}+\mathbf{Q}}} \times M^{\mathbf{G}}_{n\mathbf{K},m\mathbf{K}+\mathbf{Q}} \left[M^{\mathbf{G}'}_{n\mathbf{K},m\mathbf{K}+\mathbf{Q}}\right]^*, \tag{2}$$

where $f^n_{\mathbf{K}} = [e^{(E_n(\mathbf{K})-E_F)/k_BT} + 1]^{-1}$ is the Fermi-Dirac distribution at temperature T, $E_n(\mathbf{K})$ are the Kohn-Sham energy levels, Ω is the normalization volume, and the charge vertices M can be found in Ref. [16]. The Coulomb interaction with the surrounding supercells in the LiC_2 superlattice arrangement is excluded, as described in detail in Ref. [29]. Our results show that the surface-plasmon peaks are much more prominent if the external probe is placed outside of the lithium plane (e.g., $z_0 = L/2$).

For better understanding of the modes and their dispersions, we compare our *ab initio* DFT results with the semiclassical ones, obtained by using a simple model schematically shown in Fig. 2, where the graphene and lithium atomic monolayers are considered as two 2D conducting plates separated by distance d and described by 2D conductivities $\sigma_\pi(\omega)$ and $\sigma_\sigma(\omega)$ obtained by the Drude model

$$\sigma_n(\omega) = \frac{i\rho_n}{\omega + i\eta}; \quad n = \pi,\sigma. \tag{3}$$

The effective numbers of the charge carriers in the graphene π and the lithium σ band are calculated from the KS wave functions and energy levels as

$$\rho_n = -\frac{2}{S} \sum_{\mathbf{K}\in SBZ} \frac{\partial f(E^n_{\mathbf{K}})}{\partial E^n_{\mathbf{K}}} \left| j^x_{n\mathbf{K},n\mathbf{K}} \right|^2; \qquad n = \pi,\sigma, \tag{4}$$

where S is the normalization surface and η is the intraband damping constant. Since the system is isotropic in the x,y plane, we chose the current to be in the x direction and the expressions for the current vertices j^x can be found in Ref. [38]. The conductivities (3) can be used to calculate the noninteracting electrons response function in the long-wavelength limit for each 2D electron gas

$$\chi^0_{\pi,\sigma}(Q \approx 0,\omega) = \frac{Q^2}{i\omega}\sigma_{\pi,\sigma}(\omega), \tag{5}$$

and these can be used to construct the RPA screened response function for each 2D electron gas taking into account only the electron-electron interaction within the electron gas as

$$\chi_{\pi,\sigma}(Q,\omega) = \frac{\chi^0_{\pi,\sigma}(Q,\omega)}{1 - \frac{2\pi}{Q}\chi^0_{\pi,\sigma}(Q,\omega)}. \tag{6}$$

If we include the electron-electron interaction between the π and σ electron gases, the dispersion relations $\omega(Q)$ of the

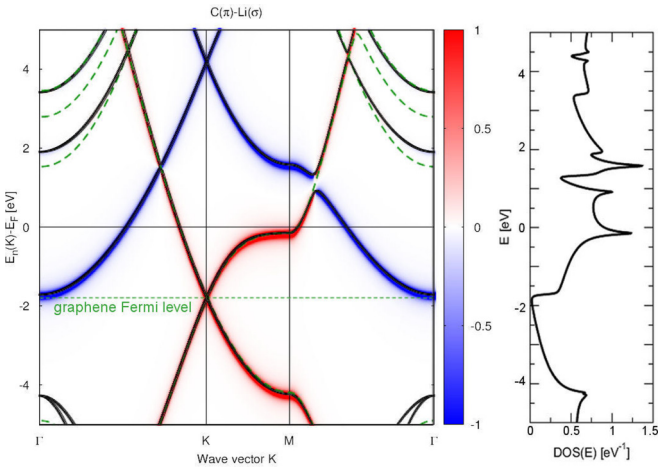

FIG. 3. The band structure and DOS of the LiC_2-ML. The color scheme is defined as the difference between the contributions of the C(π) and Li(σ) orbitals in the band structure. That is, red denotes the dominantly C(π) bands and blue denotes the dominantly Li(σ) bands. The green dashed lines show the pristine graphene band structure and Fermi level (for comparison).

coupled collective modes can be obtained from $[\frac{2\pi}{Q}e^{-Qd}]^2\chi_\pi\chi_\sigma = 1$.

In order to explore the influence of the interlayer $\pi \to \sigma$ excitations we need to improve our model by allowing the interlayer electron-hole (e-h) excitations. To achieve that, we correct the total Drude conductivity ($\sigma_\pi + \sigma_\sigma \to \sigma_\pi + \sigma_\sigma + \sigma_{\pi\sigma}$) by adding the interband term

$$\sigma_{\pi\sigma}(\omega) = \frac{-4i\hbar\omega}{S}\sum_{\mathbf{K}}\frac{(f_{\pi\mathbf{K}} - f_{\sigma\mathbf{K}})\left|j^x_{\pi\mathbf{K},\sigma\mathbf{K}}\right|^2}{\Delta_{\pi\sigma}(\mathbf{K})[(\hbar\omega + i\eta_{\pi\sigma})^2 - \Delta^2_{\pi\sigma}(\mathbf{K})]}, \tag{7}$$

where $\Delta_{\pi\sigma}(\mathbf{K}) = E_{\pi\mathbf{K}} - E_{\sigma\mathbf{K}}$. The interband term is added only to the graphene Drude conductivity ($\sigma_\pi \to \sigma_\pi + \sigma_{\pi\sigma}$) to preserve the division into two nonoverlapping layers. It could have been added to the lithium Drude conductivity, and that would lead to the same result, while adding it to both Drude conductivities would be overcounting.

Figure 3 shows the band structure and density of states (DOS). The color scheme in the band structure is used to express the difference between the contributions of the carbon π orbitals and the lithium σ orbitals in the LiC_2-ML band structure. The positive (red) values denote the dominantly C(π) bands, while negative (blue) values denote the dominantly Li(σ) bands. In addition to that, we introduce the notation π and π^* for the graphene conical bands below and above the Dirac point (at the K point), respectively, as well as σ and σ^* for the highest occupied and the lowest unoccupied parabolic lithium bands (at the Γ point), respectively. If we compare this with the band structure of the pristine graphene (green dashed lines), we can see several important differences arising from the increase of the Fermi level on one hand, and the occurrence of the new (lithium) bands on the other. Around the Γ point we can see the parabolic bands, typical for lithium, while around the K point we can see the conical bands, typical for graphene, with the Dirac point now significantly below the Fermi level.

To obtain the highly accurate spectra, and to be able to reach the long-wavelength limit, we calculate the independent electron response function (2) by using $601 \times 601 \times 1$ K-point mesh sampling which corresponds with 361 801 Monkhorst-Pack special k points in the Brillouin zone. This enables us to use a very small damping parameter $\eta = 10$ meV, which is in good agreement with the average experimental intraband damping constant [19], and achieve high resolution of our spectra without encountering numerical difficulties. This is only necessary for the very small wave vectors ($Q < 0.03$ a.u.), while for the larger Q it is sufficient to use $201 \times 201 \times 1$ K-point mesh sampling which corresponds with 40 405 Monkhorst-Pack special k points in the Brillouin zone, in which case we have to use a slightly larger damping parameter $\eta = 30$ meV, since any lower value would lead to numerical difficulties. In all cases the band summation is performed over 30 bands, which proved to be sufficient for proper description of the electronic excitations up to 40 eV. Broken inversion symmetry requires the inclusion of the crystal local field effects in the z direction, which is achieved by using $47G_z$ Fourier components, corresponding with the 20 Ry (544 eV) crystal local field effects cutoff. Excluding the crystal local field effects in the z direction would result in averaging the charge-density fluctuations in this direction which would automatically eliminate the AP from the spectra since they oscillate in antiphase. In the semiclassical models (3) and (7) the temperature is chosen to be $T = 20$ meV (230 K), which means that the effective numbers of charge carriers in the graphene π^* and lithium σ bands are $\rho_\pi = 0.042$ a.u.$^{-2}$ and $\rho_\sigma = 0.037$ a.u.$^{-2}$, respectively. The damping constant is $\eta = 10$ meV, and the separation between the conducting plates d can be used as the fitting parameter to fit the model AP to the one obtained by the RPA *ab initio* calculations. The fitting is achieved for $d = 0.75$ a.u., which may seem too small, considering that the equilibrium separation between the graphene and lithium atomic planes is 4.1 a.u., but we need to keep in mind that d is the effective distance between the two 2D plasmas and not the separation between the atomic planes. The position of the effective image plane z^{im} is the displacement of the 2D plasma with respect to the corresponding atomic plane, and in the graphene $z^{im}_\pi \approx 2$ a.u. [30]. Therefore, $d = 0.75$ a.u. means that the effective image plane in the lithium would be $z^{im}_\sigma \approx 1.35$ a.u., which is reasonable considering that the lithium σ orbitals are more localized (in the atomic plane) than the graphene π orbitals. In other words, this result suggests that the purely classical description of the two oscillating plasmas located in the Li and C atomic planes is not correct, which is a direct consequence of the importance of the quantum-mechanical dispersivity in the solid/vacuum interfacial region and also of quantum-mechanical nonlocality which is particularly important at small separations from the surface or in the case of the few nanometers large objects such as graphene nanodisks, metasurface, or nanoribbons [19,39,40].

Figures 4 and 5 present the excitation spectra in the Γ–M direction. It is important to point out that we performed the same calculations in the Γ–K direction as well, and found out that there are no significant differences, especially not in the long-wavelength limit, so we chose to present the results in the Γ–M direction only, since the Monkhorst-Pack mesh

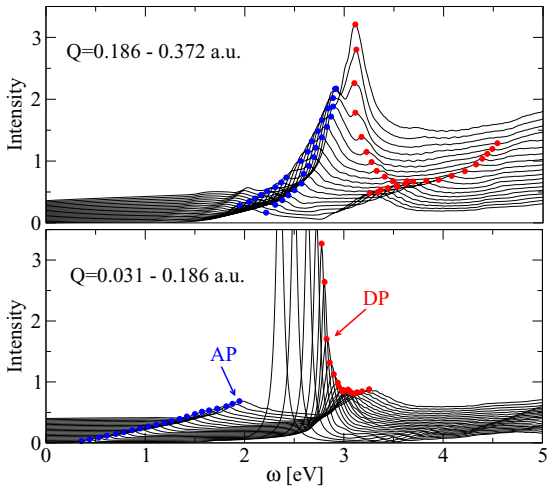

FIG. 4. The spectra of the electronic excitations for the wave vectors 0.031 a.u. $< Q <$ 0.186 a.u. (lower panel) and 0.186 a.u. $< Q <$ 0.372 a.u. (upper panel), in the Γ–M direction. Dots denote the peaks of the plasmon modes.

used in the calculations provides the highest resolution in that direction. Figure 4 shows the low-energy ($\hbar\omega < 5$ eV) excitation spectra for the wave vectors 0.031 a.u. $< q <$ 0.372 a.u. On the lower panel we can see two prominent peaks. The one with the lower frequency (denoted by the blue dots) is very weak for the small Q, but increases for the larger Q, while the other one (denoted by the red dots) is initially very strong but then rapidly decreases for the larger Q. Figure 5

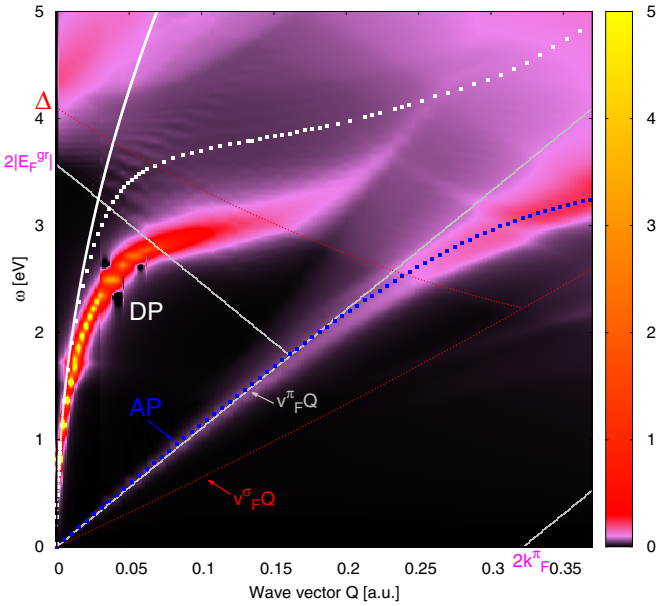

FIG. 5. The intensity of the electronic excitations in LiC_2-ML. The thick white line shows the dispersion of the DP obtained in the Drude model (3) while the dispersion relation of the AP in that model coincides with the $v_F^\pi Q$ line. The white and blue squares show the dispersion relations of DP and AP in the Drude model corrected with the interband term (7), respectively. The thin white and red lines show the boundaries of the $\pi \to \pi^*$ and $\sigma \to \sigma^*$ e-h excitation gap around the Dirac (K) point and around the Γ point, respectively (as described in the text).

shows the same spectra as the functions of the frequency and wave vector, with the intensities shown by the color scheme, which enables us to see the dispersions of the modes. For comparison, the dispersions of the plasmon modes obtained by the Drude model (3) are shown by the white lines; one thick with square-root shape, and the other thin and coinciding with the $v_F^\pi Q$ line. This enables us to identify these modes as the AP and DP. The dispersion of the DP obtained in the Drude model matches the RPA *ab initio* result only in the long-wavelength limit $Q < 0.005$ a.u.$^{-1}$, while for the larger Q's it severely overestimates it, which is reasonable because this mode is strongly affected by the interband graphene $\pi \to \pi^*$, lithium $\sigma \to \sigma^*$, and graphene-lithium $\pi^* \leftrightarrow \sigma$ excitations. The blue and white squares in Fig. 5 show the dispersion relations of the collective modes in the two plasmas model with the correction (7). We see that the AP barely changes (and only for the larger wave vectors), while the energy of the DP is significantly decreased and closer to the results obtained by the RPA *ab initio* calculations. The still present disagreement between these results for the DP for larger wave vectors Q is not surprising, since the approximation (5), valid only in the long-wavelength ($Q \approx 0$) limit, is used for all wave vectors. The more sophisticated calculation of $\sigma_n(\omega)$, for finite Q including more interband transitions, would provide better agreement. However, this is not our objective, since the purpose of this model calculation is just better understanding of these modes. Figure 5 also shows the boundaries of the $\pi \to \pi^*$ e-h excitation gap (thin white lines; one denoted as $v_F^\pi Q$ and the other starting at $2|E_F^{gr}|$) and $\sigma \to \sigma^*$ e-h excitation gap around the Γ point [thin red lines; one denoted as $v_F^\sigma Q$ and the other starting at $\Delta = 4.1$ eV, which is the difference between σ and σ^* bands at the σ band Fermi wave vector ($k_F^\sigma = 0.47$ a.u.)]. Here $v_F^\pi = 0.41$ a.u. (8.9×10^5 m/s) and $v_F^\sigma = 0.23$ a.u. (5×10^5 m/s) are the Fermi velocities in the π and σ bands, respectively, and $E_F^{gr} = -1.78$ eV is the Fermi energy of the pristine graphene with respect to the Fermi energy of the LiC_2-ML (which is the origin of the energy scale in our calculations). The spectra shown in the upper panel of Fig. 4 are more complicated, because the plasmon modes enter into the e-h excitations area, which causes splitting of the two original plasmons into four modes. As Fig. 5 suggests, at even larger wave vectors, two of these modes seem to be damped by the e-h excitations, while the remaining two are significantly increased. All this deserves a detailed analysis, including the calculations of the optical activity and the induced electrical fields of these modes, but that exceeds the scope of this Rapid Communication.

In conclusion, we performed the high-accuracy *ab initio* DFT calculations of the electronic excitation spectra in the LiC_2-ML. The presence of lithium modifies the pristine graphene band structure in a way that increases its Fermi level and contributes a new σ band which crosses the Fermi level. This transforms the graphene to a metal placed in the vicinity of another 2D metal, which enables collective and single-particle excitations not possible in the graphene monolayer (pristine or doped). The low-energy parts of the excitation spectra show two plasmons: one in-phase (Dirac plasmon) and one in-antiphase (acoustic plasmon). Intensities of both modes are very high, enabling us to predict the possibility of their experimental observation.

Both authors are grateful to M. Šunjić and I. Kupčić for useful discussions. V.D. is grateful for the hospitality at the Donostia International Physics Center (DIPC) where this work was finalized. V.D. acknowledges support from the QuantiXLie Center of Excellence.

[1] A. Kumar, A. L. M. Reddy, A. Mukherjee, M. Dubey, X. Zhan, N. Singh, L. Ci, W. E. Billups, J. Nagurny, G. Mital, and P. M. Ajayan, ACS Nano **5**, 4345 (2011).
[2] S. L. Yang, J. A. Sobota, C. A. Howard, C. J. Pickard, M. Hashimoto, D. H. Lu, S. K. Mo, P. S. Kirchmann, and Z. X. Shen, Nat. Commun. **5**, 3493 (2014).
[3] N. M. Caffrey, L. I. Johansson, C. Xia, R. Armiento, I. A. Abrikosov, and C. Jacobi, Phys. Rev. B **93**, 195421 (2016).
[4] S. Ichinokura, K. Sugawara, A. Takayama, T. Takahashi, and S. Hasegawa, ACS Nano **10**, 2761 (2016).
[5] K. Li, X. Feng, W. Zhang, Y. Ou, L. Chen, Ke. He, Li-Li Wang, L. Guo, G. Liu, Qi-Kun Xue, and X. Ma, Appl. Phys. Lett. **103**, 062601 (2013).
[6] M. Khantha, N. A. Cordero, L. M. Molina, J. A. Alonso, and L. A. Girifalco, Phys. Rev. B **70**, 125422 (2004).
[7] P. Pervan, P. Lazić, M. Petrović, I. Šrut Rakić, I. Pletikosić, M. Kralj, M. Milun, and T. Valla, Phys. Rev. B **92**, 245415 (2015).
[8] M. Jablan, H. Buljan and M. Soljačić, Phys. Rev. B **80**, 245435 (2009).
[9] F. Bonaccorso, Z. Sun, T. Hasan, and A. C. Ferrari, Nat. Photonics **4**, 611 (2010).
[10] A. Vakil and N. Engheta, Science **332**, 1291 (2011).
[11] T. Low and P. Avouris, ACS Nano **8**, 1086 (2014).
[12] C. Vacacela Gomez, M. Pisarra, M. Gravina, J. M. Pitarke, and A. Sindona, Phys. Rev. Lett. **117**, 116801 (2016).
[13] T. Stauber and H. Kohler, Nano Lett. **16**, 6844 (2016).
[14] E. H. Hwang, R. Sensarma, and S. Das Sarma, Phys. Rev. B **82**, 195406 (2010).
[15] Y. Liu and R. F. Willis, Phys. Rev. B **81**, 081406(R) (2010).
[16] V. Despoja, D. Novko, K. Dekanić, M. Šunjić, and L. Marušić, Phys. Rev. B **87**, 075447 (2013).
[17] E. H. Hwang and S. Das Sarma, Phys. Rev. B **75**, 205418 (2007); **80**, 205405 (2009).
[18] Z. Fei, G. O. Andreev, W. Bao, L. M. Zhang, A. S. McLeod, C. Wang, M. K. Stewart, Z. Zhao, G. Dominguez, M. Thiemens, M. M. Fogler, M. J. Tauber, A. H. Castro-Neto, C. N. Lau, F. Keilmann, and D. N. Basov, Nano Lett. **11**, 4701 (2011).
[19] H. Yan, T. Low, W. Zhu, Y. Wu, M. Freitag, X. Li, F. Guinea, P. Avouris, and F. Xia, Nat. Photonics **7**, 394 (2013).
[20] Marko Kralj (private communication).
[21] P. Di Pietro, M. Ortolani, O. Limaj, A. Di Gaspare, V. Giliberti, F. Giorgianni, M. Brahlek, N. Bansal, N. Koirala, S. Oh, P. Calvani, and S. Lupi, Nat. Nanotechnol. **8**, 556 (2013).
[22] S. Feng, M. C. dos Santos, B. R. Carvalho, R. Lv, Q. Li, K. Fujisawa, A. L. Elas, Y. Lei, N. Perea-Lpez, M. Endo, M. Pan, M. A. Pimenta, and M. Terrones, Sci. Adv. **2**, e1600322 (2016).
[23] A. Marini, I. Silveiro, and F. Javier Garca de Abajo, ACS Photonics **2**, 876 (2015).
[24] J. M. Pitarke, V. U. Nazarov, V. M. Silkin, E. V. Chulkov, E. Zaremba, and P. M. Echenique, Phys. Rev. B **70**, 205403 (2004).
[25] B. Diaconescu, K. Pohl, L. Vattuone, L. Savio, P. Hofmann, V. M. Silkin, J. M. Pitarke, E. V. Chulkov, P. M. Echenique, D. Farías, and M. Rocca, Nature (London) **448**, 57 (2007).
[26] V. M. Silkin, J. M. Pitarke, E. V. Chulkov, B. Diaconescu, K. Pohl, L. Vattuone, L. Savio, Ph. Hofmann, D. Farías, M. Rocca, and P. M. Echenique, Phys. Status Solidi **205**, 1307 (2008).
[27] Y. Fedutik, V. V. Temnov, O. Schöps, U. Woggon, and M. V. Artemyev, Phys. Rev. Lett. **99**, 136802 (2007).
[28] W. L. Barnes, A. Dereux, and T. W. Ebbesen, Nature (London) **424**, 824 (2003).
[29] V. Despoja, Z. Rukelj, and L. Marušić, Phys. Rev. B **94**, 165446 (2016).
[30] V. Despoja, D. J. Mowbray, D. Vlahović, and L. Marušić, Phys. Rev. B **86**, 195429 (2012).
[31] V. Despoja, K. Dekanić, M. Šunjić, and L. Marušić, Phys. Rev. B **86**, 165419 (2012).
[32] P. Giannozzi, S. Baroni, N. Bonini, M. Calandra, R. Car, C. Cavazzoni, D. Ceresoli, G. L. Chiarotti, M. Cococcioni, I. Dabo *et al.*, J. Phys.: Condens. Matter **21**, 395502 (2009).
[33] N. Troullier and J. L. Martins, Phys. Rev. B **43**, 1993 (1991).
[34] J. P. Perdew and A. Zunger, Phys. Rev. B **23**, 5048 (1981).
[35] R. Saito, G. Dresselhaus, and M. S. Dresselhaus, *Physical Properties of Carbon Nanotubes* (Imperial College Press, London, 1998).
[36] H. J. Monkhorst and J. D. Pack, Phys. Rev. B **13**, 5188 (1976).
[37] L. Marušić and M. Šunjić, Phys. Scr. **63**, 336 (2001).
[38] D. Novko, M. Šunjić, and V. Despoja, Phys. Rev B **93**, 125413 (2016).
[39] T. Christensen, W. Wang, A.-P. Jauho, M. Wubs, and N. A. Mortensen, Phys. Rev. B **90**, 241414(R) (2014).
[40] Y. Fan, N.-H. Shen, T. Koschny, and C. M. Soukoulis, ACS Photonics **2**, 151 (2015).